XVI International Conference on Computational Plasticity. Fundamentals and Applications
COMPLAS 2021
E. Oñate, D. Peric, M. Chiumenti and Eduardo de Souza Neto (Eds)

GEOMETRICALLY EXACT INTEGRAL-BASED NONLOCAL MODEL OF DUCTILE DAMAGE: NUMERICAL TREATMENT AND VALIDATION

ALEXEY V. SHUTOV[*†] AND VLADISLAV S. KLYUCHANTSEV[*†]

[*] Lavrentyev Institute of Hydrodynamics
Pr. Lavrentyeva 15, 630090 Novosibirsk, Russia

[†] Novosibirsk State University
Ul. Pirogova 1, 630090 Novosibirsk, Russia
Email: alexey.v.shutov@gmail.com - Web page: http://sites.google.com/site/materialmodeling

Key words: Large Strain, Plasticity, Ductile Damage, Nonlocal Damage, FEM, Validation

Abstract. The applicability of a previously proposed finite strain model of nonlocal damage is analyzed. The model kinematics is based on the multiplicative decomposition of the deformation gradient into three parts: porosity-induced dilatation, elastic strain, and plastic strain. The nonlocality is introduced by integral-based averaging operator, applied to the so-called continuity parameter, which is dual to porosity. Withing the advocated modelling framework, basic principles like objectivity and thermodynamic consistency are satisfied. Using a home-made FEM code, we compare simulation results with actual experimental data regarding crack initiation and propagation. The underlying problem of destruction of a plate with a hole is considered, naturally involving large inelastic deformations prior to strain localization. The plate's material is Russian structural steel 20. A quantitative comparison is carried out in terms of force-displacement curves. Experimentally measured strain distributions and crack growth are used for a qualitative validation of the nonlocal model.

1 INTRODUCTION

We develop the integral-based approach to nonlocal damage [8, 3], aiming for numerical analysis of crack initiation and propagation in metals. The starting point of the model derivation is the previously proposed phenomenological model of finite strain plasticity with damage [13]. The original local model is extended by the averaging operator [3], applied to damage-related quantities like porosity and continuity. Depending on the implemented delocalization procedure, at least one internal length parameter is introduced into the formulation. Thus, the damage localization is controlled by the presence of length-like parameters, regularizing the boundary value problem. As demonstrated in the current paper, owing to the introduced regularization, robust and physically sound FEM simulations of crack initiation and propagation are possible. We show that unphysical localization of strain and damage into a zero thickness layer, typical for local models of strain-softening materials, is effectively prevented.

The closed system of nonlocal constitutive equations, tested here, was presented and discussed in [15]. As shown in [15], model's thermodynamic consistency and objectivity hold true; for some versions of the delocalization procedure, the so-called w-invariance can be also established. Moreover, efficient numerical algorithms were proposed in [15] and the model's applicability was tested within a series of smoothed particle hydrodynamics (SPH) computations. In the current study we test the robustness of the integral-based approach from [15], being combined with fully explicit FEM. As a demonstration problem, we simulate crack initiation and propagation during stretching of a thin plate with a circular hole. The resulting force-displacement curves as well as patterns of strain and damage distribution serve the validation of the model.

2 DUCTILE DAMAGE MODEL ON THE REFERENCE CONFIGURATION

We implement a ductile damage model from [15]. Its backbone is the elasto-viscoplasic model of Simo and Miehe [16], extended to account for damage-induced porosity [14]. Originally, constitutive equations were formulated on intermediate (fictitious) configurations. However, to develop a numerical scheme, we transform the constitutive equations to the reference configuration. Thus, the local current state of the material is captured by the inelastic (plastic) right Cauchy-Green tensor $\overset{\mathrm{por}}{\mathbf{C}}_{\mathrm{i}}$, which operates on the porous configuration, the Odqvist parameter s, and the scalar porosity $\Phi \geq 1$. Limiting cases $\Phi = 1$ and $\Phi \to \infty$ correspond to the intact and the fully destroyed states, respectively.

The second Piola-Kirchhoff stress tenor, acting on the reference configuration, is given by the formula

$$\tilde{\mathbf{T}} = \frac{k(\Phi)}{10}\big((\sqrt{\det \mathbf{C}}/\Phi)^5 - (\sqrt{\det \mathbf{C}}/\Phi)^{-5}\big)\mathbf{C}^{-1} + \mu(\Phi)\mathbf{C}^{-1}(\overline{\mathbf{C}}\,\overset{\mathrm{por}}{\mathbf{C}}{}_{\mathrm{i}}^{-1})^{\mathrm{D}}, \tag{1}$$

where $\mathbf{C}$ is the local right Cauchy-Green tensor; $\overline{\mathbf{C}} = (\det \mathbf{C})^{-1/3}\mathbf{C}$ is its unimodular part; $(\cdot)^{\mathrm{D}}$ is the deviatoric part of a tensor; $k(\Phi)$ and $\mu(\Phi)$ are damage-dependent bulk and shear moduli. Note that the volumetric part of the stress response is evaluated according to the ansatz of Hartmann and Neff [5]. The deviatoric part corresponds to the neo-Hookean type. Next, we consider the Frobenius norm of the Kirchhoff stress deviator, cf. [15]. In terms of tensors operating on the reference configuration it equals

$$\mathfrak{F} = \Phi^{-1}\sqrt{\mathrm{tr}\big[\big(\mathbf{C}\tilde{\mathbf{T}}\big)^{\mathrm{D}}\big]^2}. \tag{2}$$

Then, the inelastic (plastic) flow is controlled by the evolution equation (cf. [15])

$$\frac{\mathrm{d}}{\mathrm{d}t}\overset{\mathrm{por}}{\mathbf{C}}_{\mathrm{i}} = 2\frac{\lambda_{\mathrm{i}}}{\mathfrak{F}}\Phi^{-1}\big(\mathbf{C}\tilde{\mathbf{T}}\big)^{\mathrm{D}}\,\overset{\mathrm{por}}{\mathbf{C}}_{\mathrm{i}}. \tag{3}$$

Here, $\frac{\mathrm{d}}{\mathrm{d}t}\overset{\mathrm{por}}{\mathbf{C}}_{\mathrm{i}}$ is the material time derivative of the inelastic right Cauchy-Green tensor; $\lambda_{\mathrm{i}} \geq 0$ is the scalar inelastic strain rate. Taking stress-strain relations (1) into account, the flow rule reduces to

$$\frac{\mathrm{d}}{\mathrm{d}t}\overset{\text{por}}{\mathbf{C}}_{\mathrm{i}} = 2\frac{\lambda_{\mathrm{i}}}{\mathfrak{F}}\Phi^{-1}\mu(\Phi)(\overline{\mathbf{C}}\ \overset{\text{por}}{\mathbf{C}}{}_{\mathrm{i}}^{-1})^{\mathrm{D}}\ \overset{\text{por}}{\mathbf{C}}_{\mathrm{i}}. \tag{4}$$

The inelastic (plastic) strain rate λ_{i} is given by the Perzyna law:

$$\lambda_{\mathrm{i}} = \frac{1}{\eta}\Big\langle\frac{f}{f_0}\Big\rangle^m, \quad f = \mathfrak{F} - \sqrt{\frac{2}{3}}\big[K(\Phi) + R(s,\Phi)\big]. \tag{5}$$

Here, $K(\Phi)$ is the damage dependent initial, uniaxial yield stress; $R(s,\Phi)$ is the isotropic hardening; f is the viscous overstress (the yield condition corresponds to the equation $f = 0$). The Odqvist parameter s, also known as plastic arc length, is related to the inelastic strain rate through $\dot{s} = \sqrt{\frac{2}{3}}\lambda_{\mathrm{i}}$. To be definite, we use the Voce rule of isotropic hardening:

$$R(s,\Phi) = \Phi^{-1}\frac{\gamma(\Phi)}{\beta_0}\big(1 - \exp(-\beta_0 s)\big). \tag{6}$$

Here, β_0 is the material parameter governing the saturation rate. To describe the damage-related deterioration of material strength, we assume (cf. [14, 15])

$$k(\Phi) = k_0 \cdot \mathrm{e}^{-\mathrm{BRR}\cdot(\Phi-1)}, \quad \mu(\Phi) = \mu_0 \cdot \mathrm{e}^{-\mathrm{SRR}\cdot(\Phi-1)}, \quad \gamma(\Phi) = \gamma_0 \cdot \mathrm{e}^{-\mathrm{IRR}\cdot(\Phi-1)}. \tag{7}$$

Here, k_0, μ_0, and γ_0 correspond to the undamaged state, characterized by $\Phi = 1$. Material constants BRR≥ 0, SRR≥ 0, and IRR≥ 0 govern the impact of material's porosity on the strength. They are called "bulk reduction rate", "shear reduction rate", and "isotropic (hardening) reduction rate", respectively. Since the yield strength is closely related to the isotropic hardening, we use a similar ansatz for the deterioration of the yield strength

$$K = K_0\ \Phi^{-1}\ \cdot \mathrm{e}^{-\mathrm{IRR}\cdot(\Phi-1)}. \tag{8}$$

Within the local damage model we assume that the porosity growth occurs due to nucleation of new pores and strain-controlled growth of the already existing:

$$\dot{\Phi}^{\text{local}}_{*} = A_{\text{nucl}}\lambda_{\mathrm{i}} + d_{\text{growth}}\ (\Phi - \Phi_0)\lambda_{\mathrm{i}}\exp\left(\sqrt{\frac{3}{2}}\frac{\mathrm{tr}(\mathbf{C}\tilde{\mathbf{T}})}{\sqrt{\mathrm{tr}\big[(\mathbf{C}\tilde{\mathbf{T}})^{\mathrm{D}}\big]^2}}\right). \tag{9}$$

Here, A_{nucl} and d_{growth} are material constants, describing nucleation and growth of voids; the growth term depends on the stress triaxiality. The system of local constitutive equations is closed by specifying initial conditions for s, Φ, and $\overset{\text{por}}{\mathbf{C}}_{\mathrm{i}}$.

In a number of studies, authors analyze which quantities should be subjected to averaging to obtain the desired regularization effect, cf. [4, 2]. As shown in [15], the averaging of the porosity Φ may yield unrealistic diffusion of damage. In a search for a different averaging candidate, we introduce the so-called continuity parameter Ψ, which is dual to the porosity Φ (cf. [15]):

$$\Psi = \exp\left(-\mathrm{PCR}(\Phi - 1)\right), \quad \Phi = 1 - \log(\Psi)/\mathrm{PCR}. \tag{10}$$

In these expressions, PCR>0 is a non-dimensional material parameter, called "porosity-continuity relation". The limiting cases $\Psi = 1$ and $\Psi \rightarrow 0$ correspond to intact and fully damaged states. This choice of Ψ is motivated by the creep damage mechanics [6].

In accordance with the fundamental work [3], we introduce the integral-based averaging operator:

$$G^{\text{delocalized}}(\mathbf{x}) = \int\limits_{Body} G(\mathbf{y})\alpha(\mathbf{x},\mathbf{y})d\mathbf{y}, \tag{11}$$

where $\alpha(\mathbf{x},\mathbf{y})$ is the averaging kernel, also known as delocalization kernel. In this study, *Body* is the reference configuration of the solid which coincides with its initial configuration. However, in general, *Body* may also be the current configuration [1, 15].

Constant fields must remain invariant under averaging. Therefore, the kernel must satisfy the following normalization restriction:

$$\int\limits_{Body} \alpha(\mathbf{x},\mathbf{y})d\mathbf{y} = 1, \quad \text{for all} \quad \mathbf{x} \in Body. \tag{12}$$

In this study, the normalization is identically satisfied by assuming (cf. [3]):

$$\alpha(\mathbf{x},\mathbf{y}) = \frac{\alpha_\infty(\| \mathbf{x}-\mathbf{y} \|)}{\int\limits_{Body} \alpha_\infty(\| \mathbf{x}-\mathbf{z} \|)d\mathbf{z}}, \quad \alpha_\infty(r) = c\Big\langle 1 - \frac{r^2}{h_{\text{NL}}^2} \Big\rangle^2, \tag{13}$$

where h_{NL} is the delocalization distance, also known as interaction distance; the constant multiplier $c > 0$ is irrelevant due to the normalization; $\langle x \rangle = \max(x, 0)$ is the MaCauley bracket. Loosely speaking, the averaging operator (11) corresponds to smearing the original local quantity and the special assumption $(13)_1$ prevents the delocalized quantity from diffusion beyond the boundary of the solid *Body*. Equation (13) is plausible in the three-dimension case and in thin plates (in the state of plane stress). Note that some additional considerations are needed for plane strain and axisymmetric problems.

As already mentioned, the averaging operator is applied to the continuity rate $\dot{\Psi}$, not to the porosity rate $\dot{\Phi}$, cf. [15]. This constitutive assumption brings the advantage of *damage trapping*: porosity increase at already damaged sites does not contribute to the damage of nearby particles. As shown in [15], this trapping effect helps preventing unrealistic diffusion of damage, which is a serious problem within nonlocal damage modelling. Usually, this problem is solved by *ad hoc* assumptions [9, 10, 17].

The original local model is thermodynamically consistent and its nonlocal extension inherits this useful property. Unfortunately, since the delocalization is carried out on the reference configuration, the weak invariance of consitutive equations under isochoroc change of the reference configuration is lost: the choice of the reference configuration becomes an essential constitutive assumption [12]. However, alternative nonlocal models of integral type which are still weakly invariant can be found in [15]. For such w-invariant models, any specific choice of the reference configuration can be counteracted by appropriate choice of initial conditions.

3 NUMERICAL PROCEDURE

An efficient and robust explicit/implicit time-stepping algorithm from [15] is employed. The constitutive equations presented in the previous section are implemented at each Gauss integration point. For a typical time step $t_n \mapsto t_{n+1}$ with $\Delta t = t_{n+1} - t_n > 0$ suppose that we know the current right Cauchy-Green tensor ${}^{n+1}\mathbf{C}$ and internal variables ${}^{n}\overset{\text{por}}{\mathbf{C}}_{\text{i}}$, ${}^{n}\Phi$, ${}^{n}s$ from the previous time step. We need to calculate the current internal variables ${}^{n+1}\overset{\text{por}}{\mathbf{C}}_{\text{i}}$, ${}^{n+1}\Phi$, ${}^{n+1}s$ and the stress tensor ${}^{n+1}\tilde{\mathbf{T}}$.

First, the elastic predictor step is carried out to obtain elastic constants, yield stress, and the trial second Piola-Kirchhoff stresses:

$$\mu = \mu_0 \exp(-\text{SRR}({}^{n}\Phi - 1)), \qquad k = k_0 \exp(-\text{BRR}({}^{n}\Phi - 1)), \tag{14}$$

$$K = K_0 \; {}^{n}\Phi^{-1} \; \exp(-\text{IRR}({}^{n}\Phi - 1)), \qquad \gamma = \gamma_0 \exp(-\text{IRR}({}^{n}\Phi - 1)), \tag{15}$$

$$\tilde{\mathbf{T}}^{\text{trial}} = \frac{k}{10}\big(({}^{n+1}J/{}^{n}\Phi)^5 - ({}^{n+1}J/{}^{n}\Phi)^{-5}\big){}^{n+1}\mathbf{C}^{-1} + \mu\, {}^{n+1}\mathbf{C}^{-1}(\overline{{}^{n+1}\mathbf{C}}\; {}^{n}\overset{\text{por}}{\mathbf{C}}{}_{\text{i}}^{-1})^{\text{D}}, \tag{16}$$

where the current Jacobian equals ${}^{n+1}J = \sqrt{\det({}^{n+1}\mathbf{C})}$. Within the predictor step, the trial driving force and isotropic hardening are also evaluated:

$$\mathfrak{F}^{\text{trial}} = {}^{n}\Phi^{-1}\sqrt{\text{tr}\big(({}^{n+1}\mathbf{C}\; \tilde{\mathbf{T}}^{\text{trial}})^{\text{D}}\big)^2}, \quad R^{\text{trial}} = {}^{n}\Phi^{-1}\frac{\gamma}{\beta_0}\big(1 - \exp(-\beta_0\; {}^{n}s)\big). \tag{17}$$

According to the viscosity law, the inelastic (plastic) strain rate λ_{i} is a function of the viscous overstress f:

$$f = \mathfrak{F}^{\text{trial}} - \sqrt{3/2}(K + R({}^{n}s)), \quad \lambda_{\text{i}} = \frac{1}{\eta}\langle f/f_0\rangle^m, \quad \langle x\rangle = \max(x, 0). \tag{18}$$

Further, the Odqvist parameter s and the inelastic right Cauchy-Green tensor are updated (cf. [15]):

$${}^{n+1}s = {}^{n}s + \Delta t\sqrt{2/3}\lambda_{\text{i}}, \quad {}^{n+1}\overset{\text{por}}{\mathbf{C}}_{\text{i}} = \overline{{}^{n}\overset{\text{por}}{\mathbf{C}}_{\text{i}} + \frac{2\Delta t \lambda_{\text{i}}\mu}{\mathfrak{F}^{\text{trial}}}({}^{n}\Phi)^{-1}\; \overline{{}^{n+1}\mathbf{C}}}. \tag{19}$$

The time-stepping method for the inelastic right Cauchy-Green tensor $\overset{\text{por}}{\mathbf{C}}_{\text{i}}$ utilizes the explicit update formula, reported in [13]. Derivation details are given in [15]. Finally, at each point of Gauss integration we evaluate the *local* porosity rate. More precisely, following (9) we have

$$\dot{\Phi}_{*}^{\text{local}} = A_{\text{nucl}}\lambda_{\text{i}} + d_{\text{growth}}\; ({}^{n}\Phi - \Phi_0)\; \lambda_{\text{i}}\; \exp\left(\sqrt{\frac{3}{2}}\frac{\text{tr}({}^{n+1}\mathbf{C}\; {}^{\text{trial}}\tilde{\mathbf{T}})}{\sqrt{\text{tr}\big[\big({}^{n+1}\mathbf{C}\; {}^{\text{trial}}\tilde{\mathbf{T}}\big)^{\text{D}}\big]^2}}\right). \tag{20}$$

By N denote the number of Gauss integration points within the *Body*. Let $\mathbf{X}_i$ and $\mathbf{x}_i$ be their position vectors in the referential (initial) and current states. At the i-th point, the local rate of porosity growth is denoted as $\dot{\Phi}^{\text{local}}_{*\ i}$ $(i = 1, 2, ..., N)$. Since the averaging operator (11) is applied to $\dot{\Psi}^{\text{local}}_{*}$, we have:

$$\dot{\Psi}^{\text{nonlocal}}_{*\ i} = \Big(\sum_{j=1}^{N} \alpha_\infty (r(\mathbf{X}_i, \mathbf{X}_j)) \ \dot{\Psi}^{\text{local}}_{*\ j} \ V_j \Big) / \Big(\sum_{j=1}^{N} \alpha_\infty (r(\mathbf{X}_i, \mathbf{X}_j)) \ V_j \Big). \tag{21}$$

In this equation, V_j is the volume related to the j-th integration point in the reference configuration. In the simplest case with only one integration point per element, this volume coincides with the initial volume of the element. After $\dot{\Psi}^{\text{nonlocal}}_{*\ i}$ is evaluated, the continuity and porosity are locally updated:

$$^{n+1}\Psi_i = \max(^{n}\Psi_i + \dot{\Psi}^{\text{nonlocal}}_{i} \cdot \Delta t, 10^{-8}), \quad ^{n+1}\Phi_i = 1 - \ln(^{n+1}\Psi_i)/\text{PCR}, \quad i = 1, 2, ...N. \tag{22}$$

Note that the cut-off value of 10^{-8} is introduced to prevent singularities, which are otherwise possible at the final stage of material failure.

4 NUMERICAL RESULTS AND VALIDATION

To demonstrate the applicability of the developed nonlocal framework, we simulate a crack initiation caused by large plastic strain, followed by a crack propagation. As a verification test, monotonic tension of a thin plate with a round hole is simulated. The plate's material is the Russian structural steel 20 [18].

The nonlocal damage model is implemented in a home-made fully explicit FEM code using the algorithm from the previous section. Low-order four-node elements with reduced integration (single integration point per element) are implemented. Eventual spurious hourglass modes are suppressed by a small penalty [19].

The sample geometry and boundary conditions are shown in Figure 1. A prescribed displacement is applied to rigid grips at the top and bottom edges of the plate. Since the plate is thin, plane stress state is assumed. Due to the symmetry of geometry and applied loads, we model only the right half of the plate. Since the plastic zone does not cross the vertical symmetry line, there is no need to correct the delocalization kernel. Otherwise, such a correction would be necessary to account for the symmetry condition.

The top and bottom grips are shifted in the vertical direction; the displacement of each grip equals $d = d_{max}(1 - \cos(\pi t/(2t_0)))$. Here, $d_{max} = 7$ mm. The implemented parameters of the material are summarized in Table 1. For comparison, we also carry out additional simulations with the local damage model; the local model corresponds to a vanishing delocalization distance: $h_{\text{NL}} \longrightarrow 0$.

Table 1: Material parameters of the nonlocal ductile damage model

k_0 [MPa]	μ_0 [MPa]	K_0 [MPa]	γ_0 [MPa]	β_0 [-]	η [s]	m [-]
175,000	80,760	280.0	1,850	5.05	1.0	1.0

Φ_0 [-]	A_{nucl} [-]	d_{growth} [-]	BRR [-]	SRR [-]	IRR [-]	PCR [-]	h_{NL} [mm]
1.0	0.01	1.0	20.0	20.0	30.0	1.0	2.5

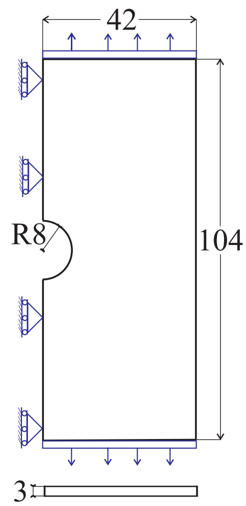

Figure 1: Thin plate with a hole: geometry, boundary conditions, and dimensions in mm. Only the right half is modelled

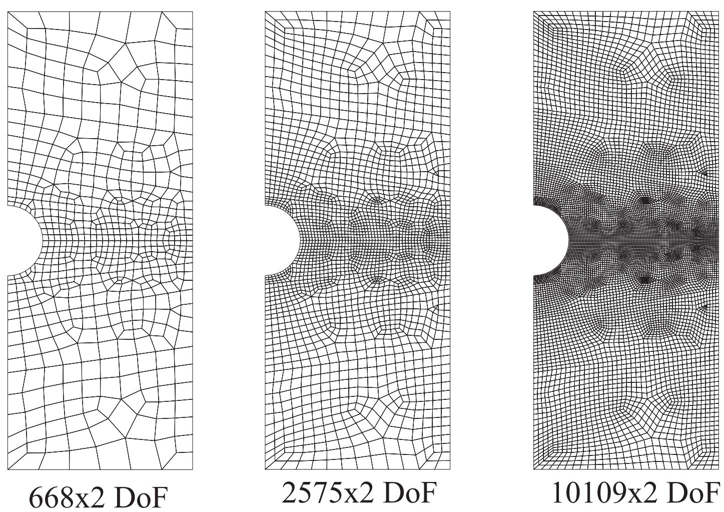

Figure 2: Three FEM meshes: coarse (left), medium (middle), and fine (right)

Three different FEM meshes are used to test the performance of the nonlocal damage model: The coarse, medium, and fine meshes have 668, 2575, and 10109 nodes, respectively (Figure 2). For the simulations based on the nonlocal model, the maximum number of delocalization neighbours ranges up to 13, 55, and 227 for the coarse, medium, and fine meshes, respectively. Figure 3 contains the simulated force-displacement curves for various meshes. Actual experimental data from [18] and results using the local damage model are also shown. As usual (cf. [3]), the local approach exhibit large scatter of simulation results: Upon mesh refinement, the mechanical response becomes non-physical with vanishing fracture toughness. In contrast to that behaviour, the new nonlocal damage model predicts consistent force-displacement curves. In terms of the peak force, the nonlocal simulations converge to a physically reasonable solution, which is close to the experimental value. Moreover, the post-peak curve exhibits a finite fracture toughness, nearly the same for all the discretizations. Animated FEM solutions are available under https://youtu.be/2u2BUhUb9nw and https://youtu.be/HlNDXMrkHOw showing the evolution of porosity and the plastic arc-length, respectively.

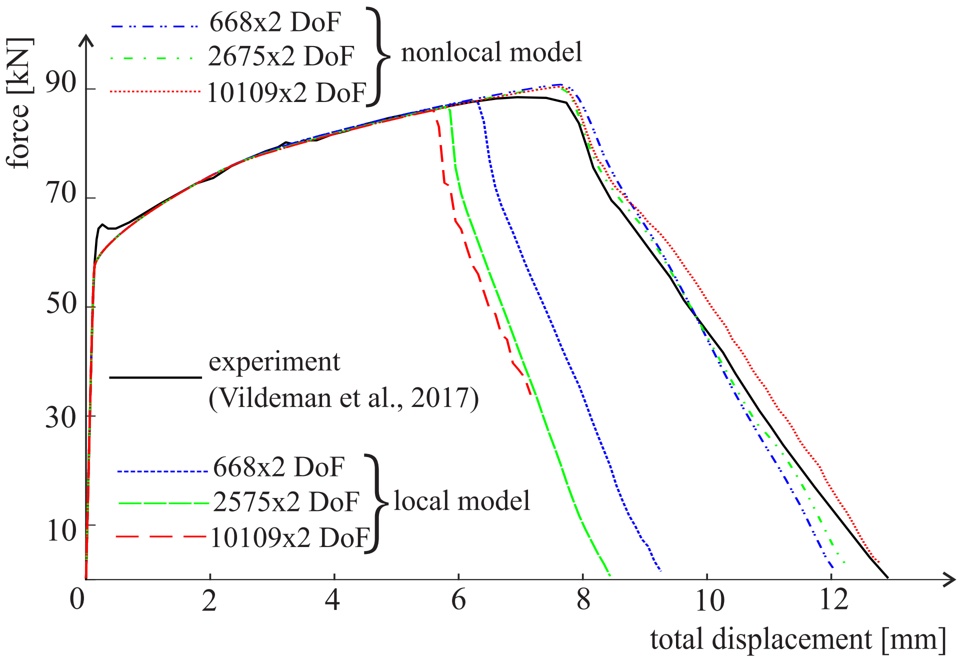

Figure 3: Simulated and experimental force-displacement curves. The experimental results are taken from [18]

Next, the experimental force-displacement curve is equipped with eight key points (Figure 4). For each key point, experimentally measured plasticity zones were reported in [18]. Namely, the outlines of the plasticity zones with 20.5 % equivalent strain are shown in Figure 5. For the validation of the nonlocal damage model, domains where the Odqvist parameter s exceeds 13% are also shown (Figure 5). The corresponding FEM simulation is carried out employing the finest mesh. The simulation results, obtained by the nonlocal model, show a strong similarity with the actual experiment: At the beginning (key points 1 to 3), FEM simulation predicts alveolous-like plastic zones. In the middle of the tension process (key points 4 to 6), the plastic zone exhibits two appendages, related to activation of two inclined shear bands. At the final stage, shortly before sample failure (key points 7 and 8) the plastic zone stretches across the entire sample. Remarkably, the actual experiment and FEM simulation are also matching in terms of the outline of the sample and the cracking pattern (Figure 6).

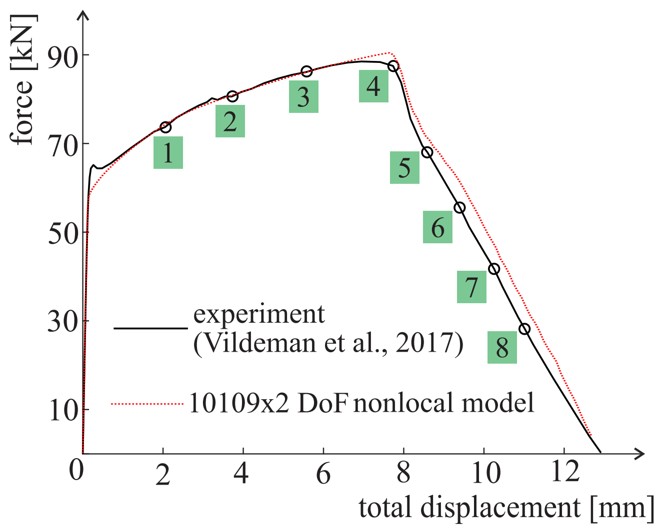

Figure 4: Force-displacment curve with eight key points, used to track zones of plasticity. The experimental curve is taken from [18]

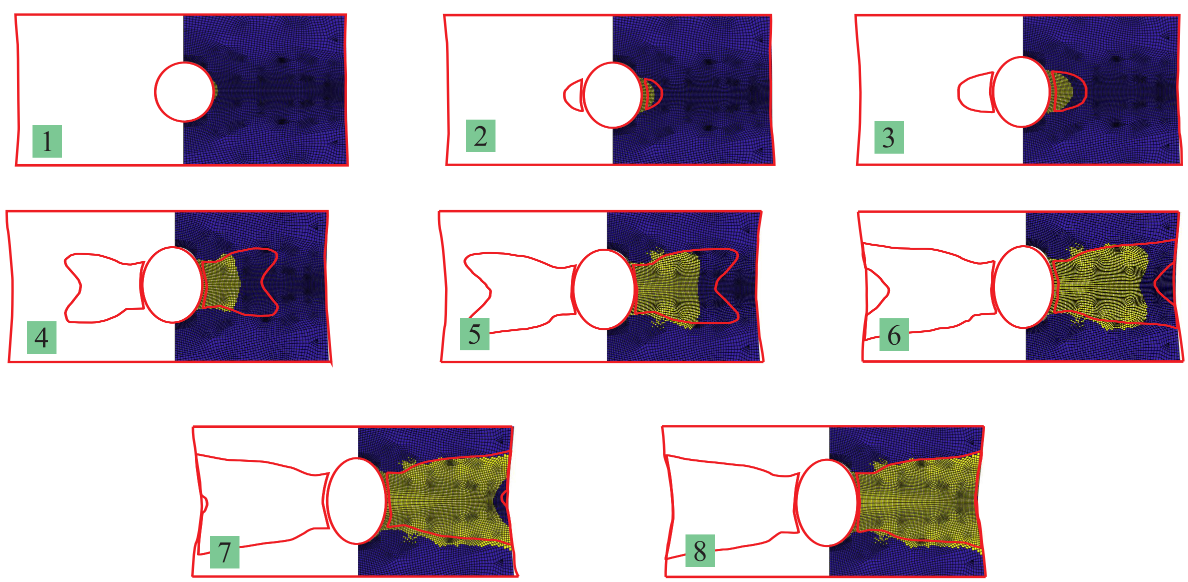

Figure 5: Distribution of plastic strain at different stages of the tension process. The red lines show the outline of the sample and of experimentally measured plastic zones. Yellow color indicates theoretical predictions of the plastic zone. Experimental data taken from [18]

Although the material parameters were only chosen to obtain a good match between experimental and theoretical force-displacement curves, the validation results are also highly satisfactory. However, one needs to keep in mind that the presented simulation results serve the demonstration of the nonlocal framework's capabilities. A proper parameter identification goes beyond the scope of this paper. Some advanced protocols of parameter identification, related to nonlocal damage models, can be found in [7, 11].

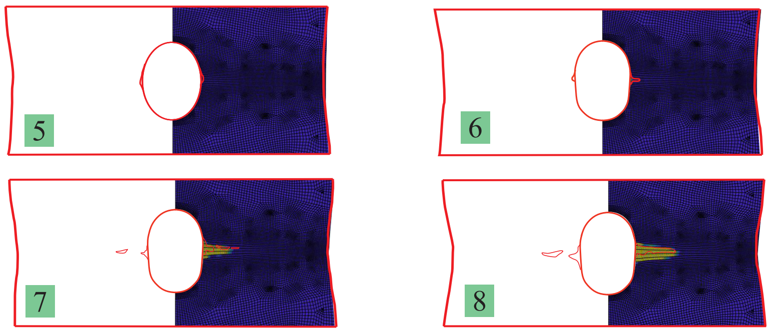

Figure 6: Experimental and theoretical cracking patterns at different stages of the loading. Yellow color indicates theoretical predictions of the macroscopic crack. Experimental data taken from [18]

5 DISCUSSION AND CONCLUSIONS

In the previous paper [15], a geometrically and physically nonlinear viscoplastic damage model was developed and implemented using smoothed particle hydrodynamics. The damage nonlocality is of integral type, where the averaging operator is applied to the continuity rate. In the current study, the applicability of the model within classical displacement-based FEM is demonstrated. Toward that end, a problem involving crack initiation after a certain amount of local plastic strain, which is followed by crack propagation, is solved numerically.

It is sown that the original local ductile damage model exhibits pathologically mesh dependent simulation results: After crack initiation, the load bearing capacity is lost almost instantly, showing unrealistically small fracture toughness of the sample. This unsatisfactory result is due to unrealistic localization of the plastic strain in a band with a vanishing thickness. Meanwhile, the nonlocal damage model from [15] predicts plausible results.

The implementation of the new nonlocal model is straightforward, when working with explicit FEM or SPH (cf. [15]). The integral-base averaging operator is highly reliable. Unlike the explicit gradient approach to nonlocality, the integral approach does not require C^1 continuous finite elements. In contrast to implicit gradient-based models, the integral approach does not require introduction of additional degrees of freedom. Due to its analytical simplicity, the integral-based approach provides a suitable entry point for microstructure-based models of ductile damage.

Acknowledgment This research was supported by the Russian Science Foundation, project number 19-19-00126.

REFERENCES

[1] Andrade, F.X.C., César de Sá, J.M.A and Andrade Pires, F.M. A ductile damage nonlocal model of integral-type at finite strains: formulation and numerical issues. *Int. J. Damage Mech.* (2011) **20**(4):515–557.

[2] Andrade, F.X.C., César de Sá, J.M.A and Andrade Pires, F.M. Assessment and comparison of non-local integral models for ductile damage. *Int. J. Damage Mech.* (2014) **23**(2):261–296.

[3] Bažant, Z.P. and Jirásek, M. Nonlocal integral formulations of plasticity and damage: survey of progress. *J. Eng. Mech.* (2002) **128**:1119–1149.

[4] Belnoue, J.P. and Korsunsky, A.M. A damage function formulation for nonlocal coupled damage-plasticity model of ductile metal alloys. *Eur. J. Mech. A Solids* (2012) **34**:63–77.

[5] Hartmann, S. and Neff, P. Polyconvexity of generalized polynomial-type hyperelastic strain energy functions for near-incompressibility. *Int. J. Solids Struct.* (2003) **40**:2767–2791.

[6] Kachanov, L.M. *Introduction to Continuum Damage Mechanics.* Springer, (1986).

[7] Nguyen, G.-D., Korsunsky, A.M. and Belnoue, J.P.-H. A nonlocal coupled damage-plasticity model for the analysis of ductile failure. *Int. J. Plast.* (2015) **64**:56–75.

[8] Ožbolt, J. and Bažant, Z.P. Numerical smeared fracture analysis: Nonlocal microcrack interaction approach. *Int. J. Num. Meth. Engng* (1996) **39(4)**:635–661.

[9] Pijaudier-Cabot, G. and Dufour, F. Non local damage model. *Eur. J. Environ. Civ. Eng.* (2010) **14**(6-7):729–749.

[10] Poh, L.H. and Sun, G. Localizing gradient damage model with decreasing interactions. *Int. J. Numer. Meth. Engng.* (2017) **110**(6):503–522.

[11] Seupel, A., Hütter, G. and Kuna, M. On the identification and uniqueness of constitutive parameters for a non-local GTN-model. *Eng. Fract. Mech.* (2020) **229**:106817

[12] Shutov, A.V. and Ihlemann, J. Analysis of some basic approaches to finite strain elasto-plasticity in view of reference change. *Int. J. Plast.* (2014) **63**:183–197.

[13] Shutov, A.V., Landrgaf, R. and Ihlemann, J. An explicit solution for implicit time stepping in multiplicative finite strain viscoelasticity. *Comput. Methods Appl. Mech. Engrg.* (2013) **265**:213–225.

[14] Shutov, A.V., Silbermann, C. B. and Ihlemann, J. Ductile damage model for metal forming simulations including refined description of void nucleation. *Int. J. Plast.* (2015) **71**:195–217.

[15] Shutov, A.V. and Klyuchancev, V.S. Large strain integral-based nonlocal simulation of ductile damage with application to mode-I fracture. *Int. J. Plast.* (2021) https://doi.org/10.1016/j.ijplas.2021.103061 .

[16] Simo, J.C. and Miehe, C. Associative coupled thermoplasticity at finite strains: formulation, numerical analysis and implementation. *Comput. Methods Appl. Mech. Engrg.* (1992) **98**:41–104.

[17] Vandoren, B. and Simone, A. Modeling and simulation of quasi-brittle failure with continuous anisotropic stress-based gradient-enhanced damage models. *Comput. Methods Appl. Mech. Engrg.* (2018) **332**(15):644–685.

[18] Vildeman, V.E., Lomakin, E.V., Tret'yakova, T.V., and Tret'yakov, M.P. Supercritical deformation and fracture of bodies with concentrators under plane stress state conditions. *Mech. Solids* (2017) **52(5)**:488–494.

[19] Wriggers, P. *Nonlinear Finite Element Methods.* Springer. Berlin-Heidelberg, (2008)